Investigating the Feasibility of Fiducial Marker Design for Pololu 3pi+ 32U4

***Abstract*—Currently, there are no fiducial markers designed specifically for the Pololu 3pi+ 32U4 robot. Fiducial markers could be helpful in line-following and maze solving tasks as they can allow the robot to localise, or change its behaviour more quickly by responding to marker codes rather than features of the natural environment. This study shows the 3pi+ 32U4 can detect different line thicknesses, allowing it to read barcodes. Additionally, the 'visual field' of each sensor, i.e. the area under each sensor within which stimuli can be detected, was defined. It was found that the robot can also detect how much of each sensor's visual field is filled with black ink, allowing it to read more complex fiducial markers. Experiments suggest there is minimal overlap between the sensor's visual fields, implicating that fiducial markers for 3pi+ 32U4 can be constructed through placing 1cm fields in a row or grid.**

I. Introduction

Fiducial markers are artificial landmarks which can signal information to a robot. These can allow the robot to localise (i.e: locate itself within a larger map) or change behaviour in other ways. Fiducial markers are typically represented by a set of patterns and accompanying computer vision algorithms to detect them [1].

A few examples of existing fiducial markers are QR codes: used in various applications to store information [2], ARTag: used in AR/VR primarily for localisation and navigation [3], and ReacTIVision: a system designed for tangible table-based interfaces [4].

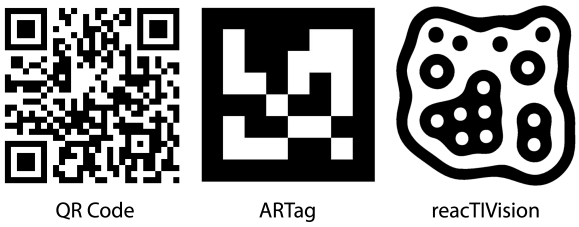

Fig. 1: Examples of existing fiducial markers.

As the Pololu 3pi+ 32U4 robot is specialised for line-following and maze-solving [5], fiducial markers could greatly enhance its navigation abilities. For example, in situations where detecting and responding to a marker is faster than detecting and responding to other natural features of the environment. Currently, there are no fiducial markers designed specifically for the 3pi+ 32U4 robot. This investigation aims to determine if it would be feasible to design fiducial markers for this robot by defining the necessary characteristics required for these fiducial markers to be operable.

The 3pi+ 32U4 has 3 central downward facing sensors [6], and it may be hypothesised that each sensor can detect stimuli within a particular area below it, which is its 'visual field.' Through testing the characteristics of each sensor's visual field, including its boundaries and sensitivity to stimuli, the design for appropriate fiducial markers can be determined. Understanding the overlap between visual fields would also help define how many isolated elements can be detected in a fiducial marker if sensors are read in parallel.

Sensors DN1 and DN5 are excluded from this investigation due to their distance from the central sensors, due to which their position changes more significantly with orientation, and their readings may be harder to compare with those of the central sensors.

Barcodes may be considered the simplest form of fiducial marker [7] as they do not require the coordinated interpretation of multiple sensors. Therefore, this investigation will first test the ability of the robot to detect barcodes, before focusing on more complex fiducial markers.

A. Hypothesis Statements

- **Hypothesis 1**: The robot can detect differences in line thickness for lines which are perpendicular to its direction of travel, therefore being able to respond to information from barcodes.
- **Hypothesis 2**: Each sensor has a visual field with boundaries that can be detected.
- **Hypothesis 3**: Each sensor can detect what proportion of its visual field is filled with black ink, allowing it to detect different patterns in its visual field.

II. Implementation

The implementation considerations for this project are minimal. In the main experiment infrared sensors DN2, DN3, and DN4 are read using a pseudo-parallel method in order to minimise overhead [8]. During preliminary work (Experiment 1) the sensors were not read in parallel. The sensor reading were taken using the recommended timing based methods from the 3PI documentations. This involves setting I/O line associated with each sensors to high, waiting 10 microseconds, then setting them to low and measuring the microseconds it takes for the voltage to decay [9]. Calibration is trial dependent due to changes in light condition between trials. The readings were then saved in a file and analysed with various techniques as seen in the results section.

III. Experiment Methodology

A. Overview of Method

1) Experiment 1 (10 repeats); Preliminary work: The first step is understanding what is the minimum width of a line that can be detected by the robot, and whether it can detect differences in line thickness. This would allow us to determine the minimum line width that can be used in any

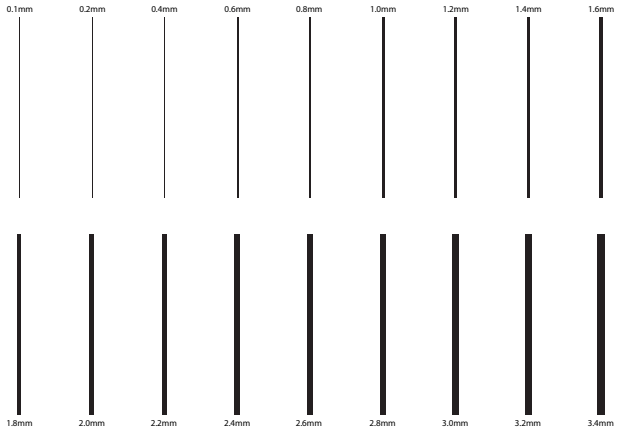

Fig. 2: Setting for Experiment 1

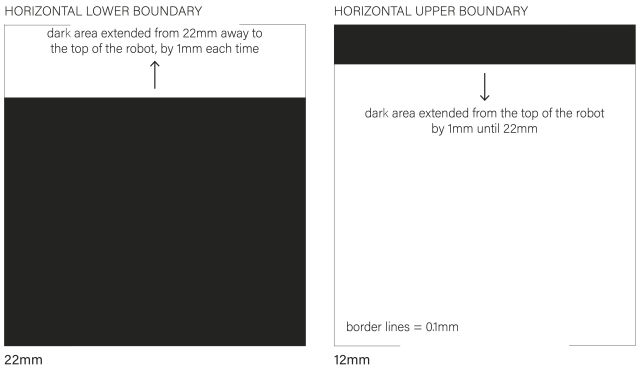

Fig. 4: Setting for experiment 2; Determining the horizontal boundaries by increasing the size of the black box by 1mm each time to cover the visual field of the sensor

barcode or marker design. It would also tell us whether the robot would be able to interpret information from barcodes perpendicular to its path by reading the thickness of each line. In order to conduct Experiment 1, the robot is moved by hand over the 2 segments in Figure 2 from left to right. Readings were taken separately for each of the 3 sensors.

2) Experiment 2 (4 trials): The second step is exploring whether the exact boundaries of each of the sensors visual fields can be determined. In order to do so we created the diagrams shown in Figure 3 and Figure 4.

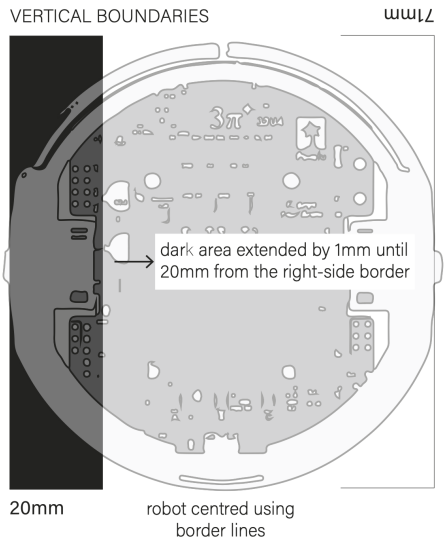

Fig. 3: Setting for experiment 2; Determining the vertical boundaries by increasing the size of the black box by 1mm each time to cover the visual field of the sensor

Between each measurement in the experiment, the black area within the box is made 1mm larger, approaching the sensors from the top, bottom, left, and right, to observe exactly where the black ink begins to be detected by each sensor.

The role of the exterior box, which is the exact size of the robot excluding the protruding axle ends, is to minimise error by being able to place the robot in the boundaries of the box. The exterior box is drawn with lines of thickness 0.1 mm, which is under the detection threshold of 0.4 mm. This ensures that the exterior box will not interfere with sensor readings during the experiment.

The horizontal range of the moving boundary is from 0 to 22mm from the top of the box, with an increment of 1mm. The vertical range is from 20mm to 71mm from the left side of the box (20mm on each side), with an increment of 1mm.

We determined those boundaries based on the measurements we took of the robot, as shown in Figure 5.

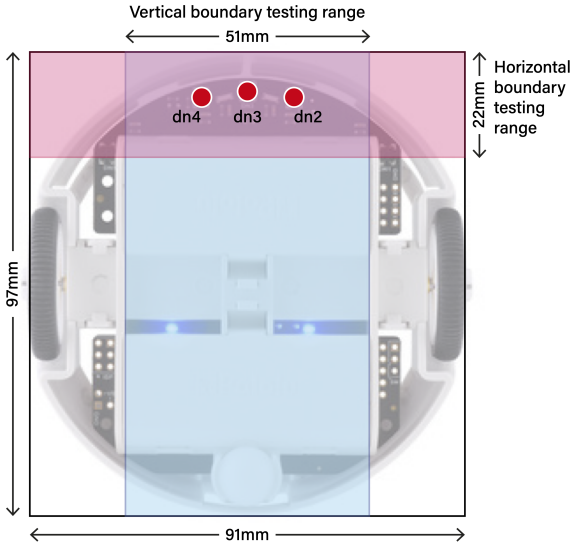

Fig. 5: Diagram showing the position of the sensors and the range in which boundaries were placed for experiment 2

In order to determine the left and right boundary of the visual fields, 2 sets of readings were taken in each vertical line box, one with the robot being placed facing the top of the box, and one with the robot facing the opposite direction.

B. Discussion of Variables

1) Experiment 1:

- Independent variable - Line thickness
- Dependent variable - Visible spike in the plotted sensor readings, indicating detection of stimulus
- Controlled variables - Intensity of lines printed, speed, and external lighting: Consistent intensity of lines

printed would allow spikes in sensor readings to be more reflective of line thickness rather than differences in intensity. Manually controlling the speed of the robot allows for a consistent rate of measurement, ensuring that perceived differences in spikes are minimally influenced by their proximity to one another. External light, i.e. sunlight, can directly contribute to noise in sensor readings due to its changing intensity throughout the day as well as the sensitivity of IR sensors [6]. Therefore the experiment are conducted with minimal natural light.

2) Experiment 2:

- Independent variable - Position of boundary stimulus
- Dependent variable - Sensor readings passing a threshold, indicating detection of stimulus
- Controlled variables - Position of robot in box, intensity of stimuli, external lighting: As the position of boundary stimuli are measured in relation to the box outline, positioning the robot consistently within the box would allow for more accurate data to be recorded. Consistent intensity of boxes printed would ensure that changes in sensor readings can be attributed to the position of the stimulus rather than its intensity. As external light can contribute to noise as discussed above, minimising its effects would allow for sensors to detect stimuli more consistently.

C. Discussion of Metrics

1) Experiment 1: To analyse the results of Experiment 1, sensor readings for each individual sensor were plotted on a graph with time on the x-axis and sensor values on the y-axis. Spikes in sensor readings were then evaluated visually to determine the earliest spike which was visually distinguishable from surrounding noise. Here, a visual approach was preferred over a quantitative approach due to the heavy presence of noise in detecting extremely thin lines. As a result, quantitative thresholds would be heavily subject to precise calibration and perfectly controlled experimental conditions.

To determine whether the robot could distinguish between line thicknesses, sensor values across line thickness values were compared to see which pairs line thickness values yielded a sensor value difference greater than 50. This difference value of 50 was chosen to be reliably detected above noise, which typically caused sensor readings to fluctuate by about 30 in our experiment.

2) Experiment 2: To analyse the results of Experiment 2, sensor values were plotted against line position: the position of the black box edge. The point at which the black box began to be detected and sensor values began to rise from the baseline was visually marked. Marked values were recorded along with the point at which 50% and 100% of the calculated visual field was filled. These were then normalised as percentage values of the maximum sensor values, and averaged so as to provide an indication of how sensor values vary as the visual field is filled. However, these values may not be directly applicable to other robots as sensor values can vary in range.

Opposite approaches of the black box, i.e: left-right and upper-lower, were plotted together to produce an estimation of each sensor's visual field, as seen in the Results section.

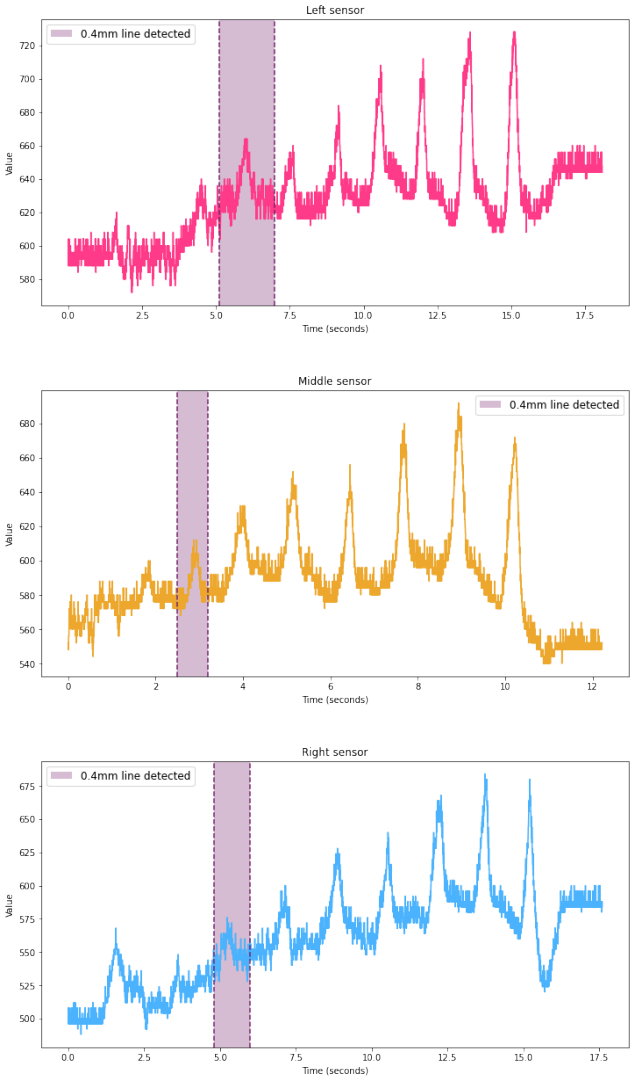

Fig. 6: Experiment 1 readings for 1 trial for the 0.1 to 1.6 mm lines; The shaded area shows the line thickness used for further experiments

IV. Results

A. Experiment 1

In Figure 6 the 0.1 mm line is showing some variation in the reading however that can be attributed to noise. While the sensor is detecting a change for the first 2 lines, those are not reliable enough to use in our future experiments as we want a clear delimitation when the robot is detecting a line.

The 0.4 mm line is clearly detected by all 3 sensors, as seen in Figure 6, with a difference of roughly 30 microseconds when the sensor is above the line.

The maximum value as the robot passes over a line is increasing with the thickness of the line. A consistent difference is showed between consecutive lines, as shown in Figure 8, which represents the means of the maximum value for each line across 10 trials. This suggests that variations in the amount that the visual field is filled directly affects the reading.

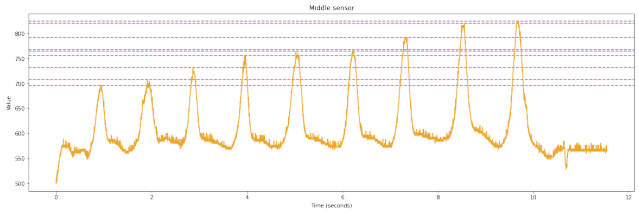

Fig. 7: Experiment 1 readings for the middle sensor (1.8 to 3.4 mm lines)

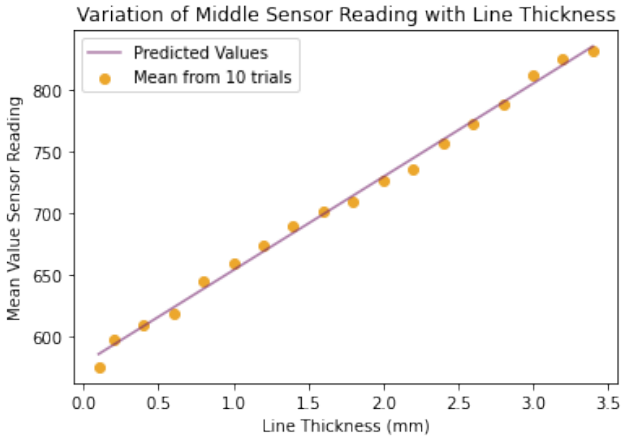

Fig. 8: Experiment 1 mean results across 10 trials; Predicted value is line of best fit

B. *Experiment 2*

Figure 9 shows the readings for the left and right boundaries for each sensors while Figure 10 show the upper and lower boundaries, those boundaries are based on the difference between mean value of the readings and the calibration value after 4 trials in the same light conditions. For both figure 9 and 10, the green lines represent the position of the sensor according to the ,documentation while the intersection of the readings for left and right boundary suggest the position of the measured centre of the visual field. In all graphs, it can be seen how around 5 mm from the sensor on each side the presence of the stimulus starts to be detected.

While the intersection of the lines does not coincide with the actual position of the sensors, the vertical errors (2.2 mm left sensor, 1.35 mm middle sensor, 0.2 mm right sensor) and horizontal errors(1.25mm left sensor, 1.66mm middle sensor, 1.6mm right sensor) are minimal (1.25 mm average vertical error, 1.5 mm average horizontal error) and can be attributed to human error when positioning the robot in the boxes. Another explanation might be a change in light due to shadows when rotating the robot for the readings. This suggest that the visual field of those sensors can be approximated to a circle with radius 1 cm, with the centre being the position of the sensors as seen in Figure 11.

Figures 9 and 10 also suggest additional information about how the extent to which the visual field of a sensor is filled affects the value of the reading. It can be seen that, as the field of vision of one sensor gets gradually filed, the value increases. Taking a closer look, Figure 13 shows the variation between the values as the visual field of the left

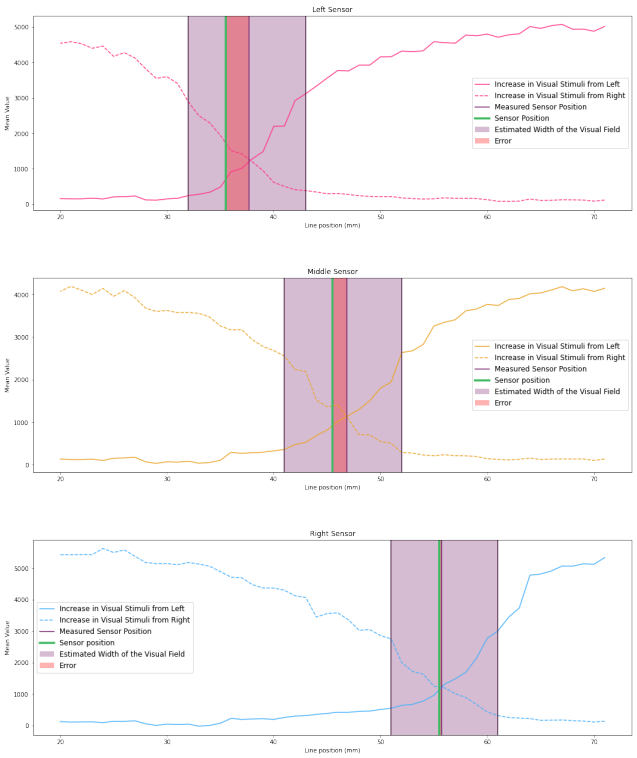

Fig. 9: Vertical boundaries determined from experiment 2; Pink is the left sensor, Yellow is the middle sensor; Blue is the right sensor

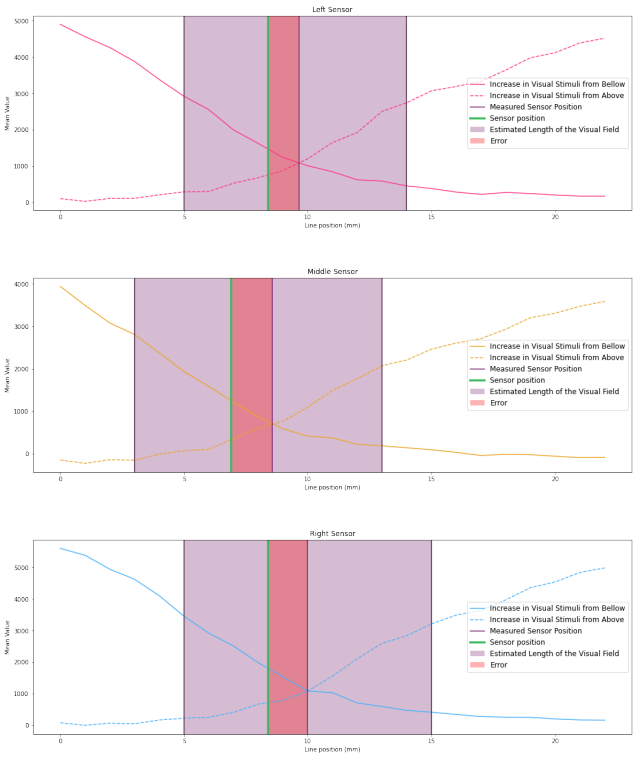

Fig. 10: Horizontal boundaries determined from experiment 2; Pink is the left sensor, Yellow is the middle sensor; Blue is the right sensor

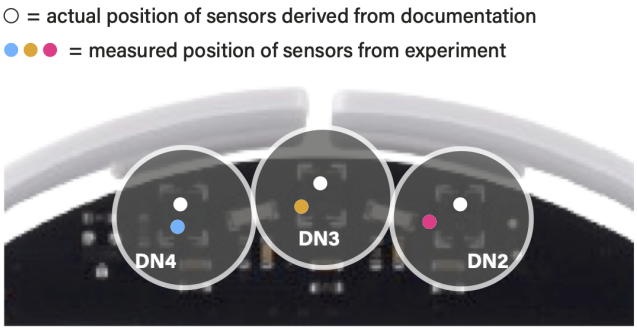

Fig. 11: Experimentally determined location of the sensors (colour) compared to real sensor position (white)

sensor is filled from the left, with readings of 1600 when the field of vision id 0% filled, 2700 for 50% and 4500 for 100%. On average at 0%, 50% and 100% of the detected visual fields being filled, the sensor values are 28.25%, 41.2% and 68.21% of the maximum values respectively, with little difference between the mean value for horizontal and vertical readings when half of the determined visual field is filled as seen in Figure 12.

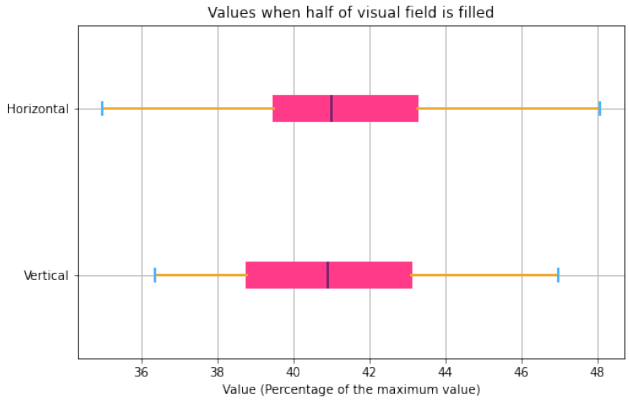

Fig. 12: Reading when the visual field is half filled; Value is represented as a percentage of the maximum value recorded

V. Discussion and Conclusion

Results will be discussed in relation to the original hypotheses.

A. The robot can detect differences in line thickness for lines which are perpendicular to its direction of travel, therefore being able to respond to information from barcodes.

Experiment 1 indicates that this hypothesis is true, as the sensor readings increase very closely in proportion to line thickness when averaged across 10 trials. However, as shown in Figure 7, line thickness differences less than 0.6 mm are not reliably detected through single passes, i.e. the difference between a 0.4 mm and 1 mm line would be detected in a single pass whereas the difference between a 0.5 mm and 0.7 mm line would not. This implicates that barcodes designed for 3pi+ 32U4 need to account for this minimum difference.

Additionally, the lines in Experiment 1 were placed approximately 35mm apart from one another, which minimised the likelihood of multiple lines being simultaneously detected. Experiment 3 suggests that each sensor's visual field spans a radius of approximately 1cm, indicating that barcodes designed for 3pi+ 32U4 should contain lines spaced at least this distance. However, as visual field boundaries have a margin for error, further experimentation to determine the minimum distance between lines that allows for isolated detection may be beneficial.

In Experiment 1, the robot was moved by hand at an approximately constant speed, which may be different to the speed typically used in line following or maze solving tasks, which has been recommended to be 0.75m/s - 1.13m/s [10]. To better account for the conditions of these tasks, barcode design should also consider how reliably they can be detected at these speeds.

B. Each sensor has a visual field with boundaries that can be detected.

Experiment 3 indicates that this hypothesis is partially true, as there are points at which the sensor readings begin to increase from baseline values, which indicate that stimuli begin to be 'seen' by the sensor as they enter its visual field.

With the assumption that visual fields are symmetrical and circular, it is possible to estimate that the boundaries of each visual field are represented by a circle of 5mm radius around each sensor. However, the assumption that the visual field is circular may be incorrect. In order to test this assumption, stimulus approaches to the sensor from all angles should be considered alongside the horizontal and vertical.

While the boundaries can be detected, it appears they cannot be sharply defined as there are no abrupt changes in the gradient of sensor readings. Therefore, there is a margin for error in defining the exact position of visual field boundaries. This is likely due to the fact that the sensor readings are based on reflection and "strongly affected by ambient light sources" [6]. While all trials in experiment 3 were conducted in the same room with closed blinds, it is still likely that the small amount of changing natural light contributed to the noise in our data. Additionally, the room had strong overhead lighting, and sensor values may have been influenced by the minor changes in robot position in relation to the lights.

Overall, this hypothesis has allowed for a broad understanding of the nature of 3pi+ 32U4 sensor visual fields; while stimuli within the visual fields can be clearly detected, its boundaries are difficult to define precisely.

C. Each sensor can detect what proportion of its visual field is filled with black ink, allowing it to detect different patterns in its visual field.

As shown in Figure 13, Experiment 3 indicates that sensor readings increase in value in proportion to the visual field being filled with stimuli. Therefore, there is a reliable difference in sensor readings when the visual field is 0%, 50%, or 100% filled. This implicates that each sensor can reliably detect *at least* 3 distinct states based on its visual stimulus. Whilst it is possible that a larger number of distinct states can be detected by filling different proportions of the visual field (e.g: 5 distinct states by filling 0%, 25%, 50%, 75%, and 100%), this represents a reliable starting point for fiducial marker design.

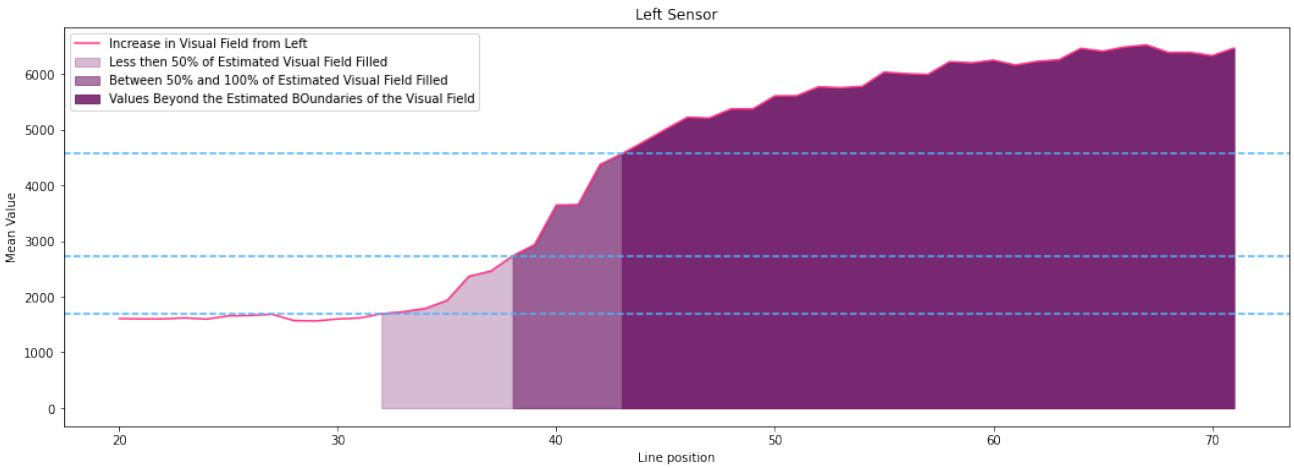

Fig. 13: Left boundary of the left sensors determined from experiment 2; Increase in reading value with increase in black in the visual field; The 50% was taken as the determined middle point of the visual field

By reading DN2, DN3, and DN4 in parallel, 27 distinct states can be detected, as shown in an example in Figure 14.

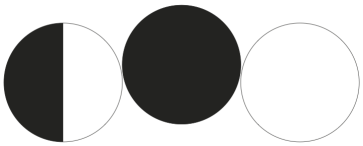

Fig. 14: Simple fiducial marker core

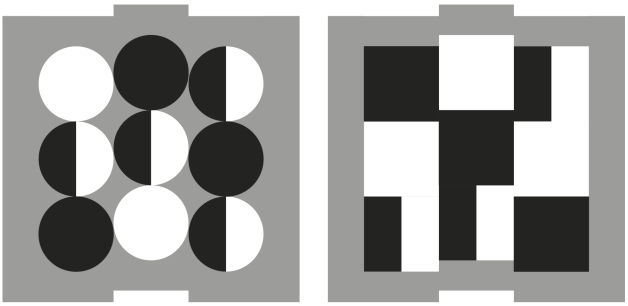

Fig. 15: Speculative fiducial marker examples

Using a 3 x 3 grid, 3^9 = 19683 distinct fiducial markers could be designed. While experiment 3 shows that 3pi+ 32U4 can reliably detect the individual rows of a 3 x 3 grid when stationary, it must be further investigated whether the entire grid can be accurately interpreted at speed.

Existing fiducial marker systems typically utilise an unbroken outline or some other uniform characteristic to allow computers to distinguish markers from the normal environment [3]. As this feature has not been investigated at the level of this study, a gray outline has been used as a speculative placeholder.

Figure 15 shows a potential first draft of fiducial markers for 3pi+ 32U4. However, these contain several features that need to be independently verified and designed further. Firstly, it is unclear whether circular or square cells would operate more effectively as the shape of visual fields was not determined. Using circular fields in initial drafts of fiducial markers may minimise overlapping detection of cells.

Fiala [1] outlines 11 evaluation criteria for fiducial markers in 3D space, 8 of which may apply to markers for 3pi+ 32U4; these are false positive rate, inter-marker confusion rate, false negative rate, minimal marker size, marker library size, immunity to lighting conditions, immunity to occlusion, and speed performance. To develop fiducial markers for 3pi+ 32U4 further, future work can analyse sensor responses to these designs and modify them to perform better against Fiala's evaluation criteria.

D. Conclusion:

Experiments conducted in this study indicate that it is possible to design fiducial markers for the 3pi+ 32U4, as it can detect line thickness greater than or equal to 0.4mm, and can detect when each sensor's visual field is 0%, 50%, or 100% filled. Further research can aim to determine (1) the shape of visual fields by analysing stimulus approaches from different angles, (2) the optimal design of fiducial marker outlines or uniform characteristics, which allow the robot to process when a marker has been encountered, (3) how the fiducial marker design for 3pi+ 32U4 can be improved to perform better in Fiala's evaluation criteria.

REFERENCES

[1] M. Fiala, "Designing highly reliable fiducial markers," *IEEE Transactions on Pattern Analysis and Machine Intelligence*, vol. 32, no. 7, pp. 1317–1324, 2010.

[2] T. J. Soon, "Qr code," *synthesis journal*, vol. 2008, pp. 59–78, 2008.

[3] M. Fiala, "Artag, a fiducial marker system using digital techniques," in *2005 IEEE Computer Society Conference on Computer Vision and Pattern Recognition (CVPR'05)*, vol. 2, pp. 590–596 vol. 2, 2005.

[4] R. Bencina, M. Kaltenbrunner, and S. Jorda, "Improved topological fiducial tracking in the reactivision system," in *2005 IEEE Computer Society Conference on Computer Vision and Pattern Recognition (CVPR'05)-Workshops*, pp. 99–99, IEEE, 2005.

[5] Pololu, "Pololu 3pi robot quick-start sheet," 2008.

[6] Pololu, "Pololu 3pi+ 32u4 user's guide," 2022.

[7] C. Scheirer and C. Harrison, "Dynatags: Low-cost fiducial marker mechanisms," in *Proceedings of the 2022 International Conference on Multimodal Interaction*, pp. 432–443, 2022.

[8] P. O'Dowd, "Labsheet 3: Line sensors," 2024.

[9] Pololu, "Pololu qtr reflectance sensor application note," 2022.

[10] H. Garnier and M. Jha, "Line tracking control and line maze solving strategies for the 3pi+ mobile robots," 2024.